Title

A comprehensive characterization of ice nucleation by three different types of cellulose particles immersed in water: lessons learned and future research directions

Supplemental Information

S.1. Particle and residual size distribution measurements

Particle size distributions of all three cellulose types over the range from 0.01 to 16 µm in diameter (D_p) were characterized in the AIDA chamber. For MCC, we analysed the average size distribution of nine different AIDA experiments (INUIT06_1, 17, 31, 42-46 and 54). During the measurements, we occasionally observed new particle formation events in the vessel (the source is not known). Accordingly, the contributions from these particle formations (D_p < 50 nm) were removed and not included in any of our analyses. For FC, two AIDA experiments (INUIT06_6 and 14) were characterized. For NCC, a total of four AIDA experiments (INUIT08_6, 7, 9 and 10) were analyzed to estimate the average size distribution.

For particle injection, dry ground MCC and FC were injected directly into the AIDA chamber using the rotating brush generator (PALAS, RBG1000). Unlike MCC and FC, wet particle generation (dispersion of 0.14 wt% NCC suspension by means of a compressed air atomizer) was employed for NCC. A custom-built atomizer, which is similar to TSI 3076 but without a vertical orifice and with an additional liquid drain bottle independent of an aqueous liquid feeding bottle (*Wex et al.*, 2015), was used for atomization. When we change the sample type examined, all components of a rotating brush generator were disassembled, washed with distilled water and dried in a drying oven to prevent carryover of sample residues into the next sample. Prior to each particle loading, aerosol-free dry synthetic air was passed through the RBG for >30 minutes. We confirmed that the background aerosol concentration was typically ~0.1 cm^{-3} in the AIDA vessel.

After the completion of injection, number and size of polydisperse cellulose particles were measured using a scanning mobility particle sizer (SMPS; TSI Inc., Model 3081 differential mobility analyzer, DMA, and Model 3010 condensation particle counter, CPC) and an aerosol particle sizer (APS; TSI Inc., Model 3321). With given combination, a wide range of size measurements (0.01 to 16 µm assuming all particles are spherical) was realized. A unit dynamic shape factor (DSF, H15a) and the particle density values reported in **Table 1** were used to obtain the geometric-based volume equivalent diameter (D_{ve}) from an APS. We note that our size distribution measurements were carried out only prior to the AIDA expansion experiment since both an SMPS and an APS were pressure sensitive and not able to run while altering sampling pressure in the chamber vessel.

Size distributions of suspended residuals derived from 5 µL of 0.03 wt% suspension were characterized using a scanning electron microscope (SEM, FEI, Quanta 650 FEG). With given concentration and droplet size, we simulated the condition of >100 particles contained in a single droplet, which is unique in the aqueous suspension experiments as compared to the dry dispersion measurements (i.e., presumably single particle per droplet condition). To minimize the inclusion of aggregates in the bulk suspension, we placed the bulk suspension in an ultrasonic bath (>40 kHz) for ~15 min prior to generating a droplet. Followed by pipetting a 5 µL droplet containing cellulose materials on 47 mm membrane filters (Whatman® Nuclepore™ Track-Etched Membranes, 0.2 µm pore size), all water content on the membrane filter was removed under a quasi-vacuum condition in a SEM chamber. After that, their residual size distributions in 2-D area equivalent diameter (D_a, >0.3 µm) were measured by assessing the Everhart-Thornley Detector (ETD) images. With this methodology, we conducted the below-the-lens image acquisition for a total of 3,761, 371 and 610 residuals of MCC, FC and NCC, respectively. The method used to derive SEM-based specific surface area (*SSA*) using residuals from 0.03 wt% suspension droplets is valid. At this concentration, the *SSA* of residuals is almost same as that of bulk dry powders (not shown). We confirm this for both MCC and FC. Note that, as the NCC sample is available only in a water-suspended form, we cannot conduct the dry powder versus residual comparison for NCC. Drying suspensions out will cause particles to be drawn together into aggregates. Nonetheless, our SEM observations suggest that the abundance of NCC aggregates is much less as compared to MCC and FC (**Sect. 4.4**). Aggregates may also be present in the suspension as mentioned in **Sect. 4.3.3**. In addition, the degree of agglomeration might be depending on the suspension concertation used to generate droplets. Our attempts to utilize the dynamic light scattering technique (NanoSight NS300, Malvern Panalytical) to measure the cellulose particle size distributions and associated *SSA* in aqueous suspension as a function of wt% were not successful. Nonetheless, the future study has to follow to constrain the SEM-based *SSA* and provide more method specific values (see **Sect. 3.1** for more details). A more precise and accurate normalization to the surface area might be the key to constrain the ice nucleation active surface-site density concept.

To ensure the similarity of abovementioned two size metrics (i.e., D_{ve} and D_a) and to further validate the size distribution measurements of an SMPS and an APS, an additional assessment of particle size distributions of dispersed particles was performed. Specifically, we analyzed particles that were collected on the filter directly from the AIDA chamber vessel. Using an SEM, D_a of 503 MCC particles as well as 154 NCC particles collected on either a 47 mm Nuclepore substrate or a copper microscopy substrate were measured to compare to the SMPS/APS size distributions.

Representative normalized surface area distributions (scaled to the total surface areas) of all cellulose particles obtained from the AIDA measurements and droplet residuals are shown in **Fig. S1**. As seen in this figure, the surface area distributions of MCC and FC particles exhibits its mode diameter (μ) of ~1 µm with a negligible contribution of particles smaller than 0.1 µm diameter (**Figs. S1a** and **S1b**). This dominance of supermicron particles to the total surface area is unique for MCC and FC. In contrast, the NCC particle surface area distribution is dominated by submicron particles with μ ~0.2 µm D_{ve} (**Fig. S1c**).With a minimum particle concentration detection limit of 0.001 cm^{-3}, the largest MCC and FC particle measured by an APS was ~10 µm in D_{ve}. This value is comparable to our previous measurement at MRI-DCECC as shown in Fig. S2 of H15a despite the shift in μ (2.22 µm for previous study). The observed shift may be due to the difference in the cut-size of inertial cyclone impactor stages (D_{50} vary in the range of ~1 to 5 µm). For clarity, the size distribution of MCC measured at MRI-DCECC is overlaid on top of that of AIDA in **Fig. S1a**. Comparing MCC to FC, the mode diameter, μ, of MCC of 1.22 µm is slightly larger than that of FC (μ = 1.13 µm). Interestingly, a similar lognormal distribution width, σ, of ~0.6 is observed for all cellulose particles (0.62, 0.60 and 0.59 for MCC, FC and NCC) regardless of difference in particle generation methods.

As shown in **Fig. S1**, the size of residuals invariably shifts towards the large size for all sample types when compared to that of aerosolized particles. The mode diameter of MCC, FC and NCC residuals (54.24, >65 and 2.68 µm) is at least an order magnitude higher as compared to that of the AIDA chamber-dispersed particles (1.22, 1.13 and 0.21 µm). Our observation of μ > 65 µm for FC suggests that this particular cellulose type tends to agglomerate in water or the original product comes in an agglomerated form in comparison to two other cellulose materials. Moreover, the spectral distribution width of residuals is a lot wider (1.26 and 0.84 for MCC and NCC, respectively) when compared to that of particles (0.62 and 0.59 for MCC and NCC, respectively). Further, the resulting ratio of the total surface to the total mass of residuals (**Table 1**) is up to two orders of magnitude less than that of particles. Overall, these observations suggest that particles in droplets may agglomerate in the presence of multiple particles in a single droplet, altering surface properties (i.e., *SSA*) and perhaps IN efficiency (*Emersic et al*., 2015; *Beydoun et al*., 2016).

In addition, our results of comparing D_{ve} to D_a (not shown) indicate the similar size distribution parameters (μ_{MCC} ~1.87 µm D_a and μ_{NCC} ~0.29 µm D_a) regardless of difference in particle generation methods. Though the spectral widths were slightly narrower (σ_{MCC} ~ 0.49 and σ_{NCC} ~ 0.40), observed similarity verifies the validity of our size distribution measurements.

References

Beydoun, H., Polen, M., and Sullivan, R. C.: Effect of particle surface area on ice active site densities retrieved from droplet freezing spectra, Atmos. Chem. Phys., 16, 13359–13378, doi: https://doi.org/10.5194/acp-16-13359-2016, 2016.

Emersic, C., Connolly, P. J., Boult, S., Campana, M., and Li, Z.: Investigating the discrepancy between wet-suspension- and dry-dispersion-derived ice nucleation efficiency of mineral particles, Atmos. Chem. Phys., 15, 11311–11326, doi: https://doi.org/10.5194/acp-15-11311-2015, 2015.

Wex, H., Augustin-Bauditz, S., Boose, Y., Budke, C., Curtius, J., Diehl, K., Dreyer, A., Frank, F., Hartmann, S., Hiranuma, N., Jantsch, E., Kanji, Z. A., Kiselev, A., Koop, T., Möhler, O., Niedermeier, D., Nillius, B., Rösch, M., Rose, D., Schmidt, C., Steinke, I., and Stratmann, F.: Intercomparing different devices for the investigation of ice nucleating particles using Snomax® as test substance, Atmos. Chem. Phys., 15, 1463–1485, doi: https://doi.org/10.5194/acp-15-1463-2015, 2015.

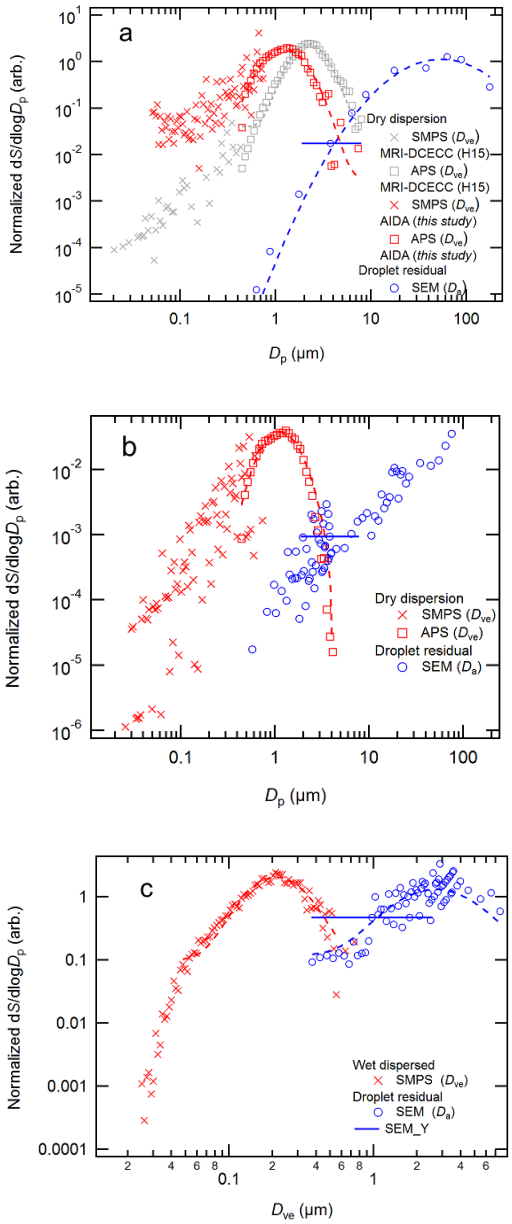

Figure S1. Surface area distributions of MCC (a), FC (b) and NCC (c) particles (red) and residuals (blue). Dry dispersed particle size distributions of MCC and FC as well as atomizer-dispersed NCC size distributions were measured by a combination of an SMPS (0.01 to 0.8 μm) and an APS (0.4 to 16 μm). The APS data of atomizer-dispersed NCC is not shown because the measured particle counts hovered around the minimum detection limit of an APS (0.001 cm^{-3}). Size distributions of droplet residuals of each particle type were measured using the off-line SEM analysis (as small as 0.3 μm). All data points

represent the particle surface area distributions normalized to the total surface area concentration. The dashed lines on SMPS and APS data points represent the lognormal fits [i.e., $y_0 + A \exp(-1(\ln(x/\mu)/\sigma))$] for >85 nm D_{ve} and >0.5 µm D_{ve}, respectively. The x-axis error bar on a selected SEM data point reflects the range of uncertainty in the particle size derived from the average aspect ratio of each particle type (i.e., 2.05, 2.03 and 2.62 for MCC, FC and NCC, respectively, from an electron micrograph). Note that both axes are in the log scale.

S.2. Log average supplement

Figure S2 shows the log average of three cellulose materials used in this study (i.e., *T*-binned log average data from **Fig. 4. iv** for MCC, FC and NCC). Reference immersion freezing $n_s(T)$ spectra for MCC (H15a) are also shown (See **Sect. 4.1**).

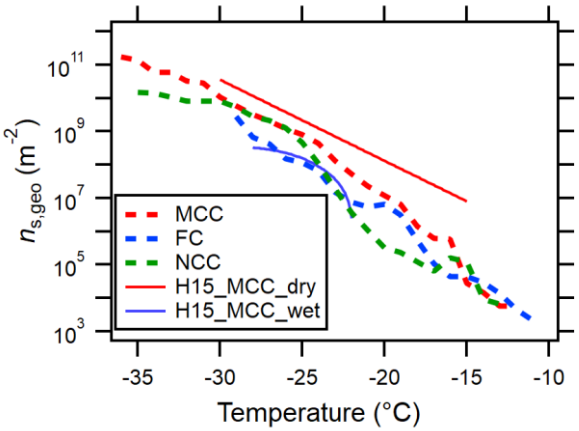

Figure S2. The *T*-binned log average of INAS density for MCC, FC, NCC. Reference immersion freezing $n_s(T)$ spectra are provided as in **Fig. 6**.

S.3. AIDA supplement

Figure S3 summarized the AIDA experiments with MCC, FC, NCC01 and NCC02. The figure is provided in support of the statements made in the Section 4.3.8, which is not evident from the compressed Figures in the main text.

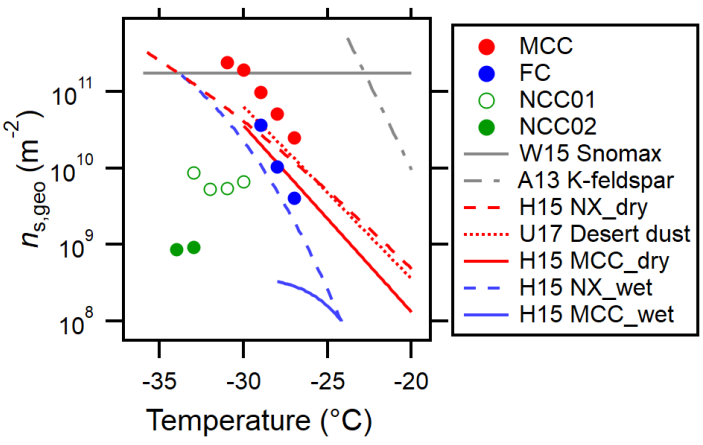

Figure S3. Derived INAS density for MCC, FC, NCC01 and NCC02. Reference immersion freezing $n_{s,geo}(T)$ spectra are provided as in **Fig. 6**. Note that the uncertainties at each data point with respect to temperature and $n_{s,geo}(T)$ are ± 0.3 °C and ± 35%, respectively (**Table 3**).

S.4. NC State-CS supplement

Figure S4 summarized the NC State experiments with FC, MCC, and NCC. The figure is provided in support of the statements made in the Section 4.3.18, which is not evident from the compressed Figures in the main text.

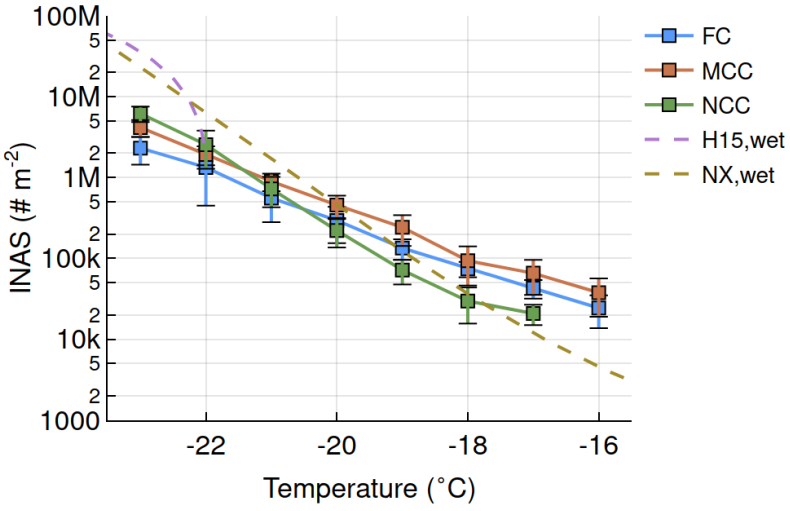

Figure S4. Derived INAS density for FC, MCC, NCC with parameterizations $n_{s,\mathrm{geo}}^{H15MCC,wet}$ and $n_{s,\mathrm{geo}}^{H15NX,wet}$ superimposed.